Median filters as a tool to determine dark noise thresholds in high resolution smartphone image sensors for scientific imaging

Damien P. Igoe,[1,2,a)] Alfio V. Parisi,[1] Abdurazaq Amar,[1] and Katherine J. Rummenie[1]
[1]*Faculty of Health, Engineering and Sciences, University of Southern Queensland, Toowoomba, Australia*
[2]*School of Medicine and Dentistry, James Cook University, Townsville, Australia*

(Received 21 September 2017; accepted 17 December 2017; published online 5 January 2018)

An evaluation of the use of median filters in the reduction of dark noise in smartphone high resolution image sensors is presented. The Sony Xperia Z1 employed has a maximum image sensor resolution of 20.7 Mpixels, with each pixel having a side length of just over 1 μm. Due to the large number of photosites, this provides an image sensor with very high sensitivity but also makes them prone to noise effects such as hot-pixels. Similar to earlier research with older models of smartphone, no appreciable temperature effects were observed in the overall average pixel values for images taken in ambient temperatures between 5 °C and 25 °C. In this research, hot-pixels are defined as pixels with intensities above a specific threshold. The threshold is determined using the distribution of pixel values of a set of images with uniform statistical properties associated with the application of median-filters of increasing size. An image with uniform statistics was employed as a training set from 124 dark images, and the threshold was determined to be 9 digital numbers (DN). The threshold remained constant for multiple resolutions and did not appreciably change even after a year of extensive field use and exposure to solar ultraviolet radiation. Although the temperature effects' uniformity masked an increase in hot-pixel occurrences, the total number of occurrences represented less than 0.1% of the total image. Hot-pixels were removed by applying a median filter, with an optimum filter size of 7×7; similar trends were observed for four additional smartphone image sensors used for validation. Hot-pixels were also reduced by decreasing image resolution. The method outlined in this research provides a methodology to characterise the dark noise behavior of high resolution image sensors for use in scientific investigations, especially as pixel sizes decrease. *Published by AIP Publishing.*
https://doi.org/10.1063/1.5006000

INTRODUCTION

Scientific applications of digital photography have been rapidly growing since the invention of the digital camera in 1974 by Steven Sasson (Präkel, 2010). The incorporation of miniaturised complementary metal oxide semiconductor (CMOS) digital imaging sensors into smartphones that have had a rapid uptake of usage by the general population provide an accessible tool for participation in citizen science projects (Hussain *et al.*, 2016a and Hussain *et al.*, 2016b), in part addressing the increasing necessity for integrated low-cost sensing (Batistell *et al.*, 2014). Smartphone camera sensors have been successfully employed in continuous remote environmental monitoring, detection of environmental contamination, subatomic particle detection, biosensing platforms, personal health monitoring, water turbidity, fluoride and salinity detection and monitoring, ultraviolet-A (UVA) aerosol optical depth evaluation, and ultraviolet-B (UVB) radiation monitoring (Hussain *et al.*, 2017; Igoe *et al.*, 2017; Park *et al.*, 2017; Turner *et al.*, 2017; Hussain *et al.*, 2016a; Hussain *et al.*, 2016b; Pérez *et al.*, 2016; Fung and Wong, 2016; Fontaine, 2015; Igoe *et al.*, 2014; Wei *et al.*, 2014; Yetisen *et al.*, 2014; and Lee *et al.*, 2012).

Any scientific image sensor-based application requires calibrating the sensor to identify any factors affecting its functionality and determine its potentials and limitations (Riutort-Mayol *et al.*, 2012). The recent trend in reducing pixel sizes and backside illumination (Chapman *et al.*, 2017; Chapman *et al.*, 2016; and Fontaine, 2015) has resulted in an increase in resolution and low-light sensitivity, providing the potential for more sensitive scientific measurements (Hussain *et al.*, 2017; Park *et al.*, 2017; Hussain *et al.*, 2016a; and Hussain *et al.*, 2016b). However, the higher resolutions have resulted in an increase in image noise, particularly "hot pixels" (Chapman *et al.*, 2016). Image sensor noise is due to the corrupted pixels that break the regular pattern of the pixel mosaic (Präkel, 2010), and it is always present in any image as it is either associated with the electronics of the sensor system, long exposure times, and object bidirectional reflectance or occurs during the image processing pipeline (Riutort-Mayol *et al.*, 2012). In general, image sensor noise could also be caused by charge leakage between pixels (Aranda *et al.*, 2017 and Riutort-Mayol *et al.*, 2012) such as the increase in impulsive noise associated with low light imaging (Aranda *et al.*, 2017; Zhu and Huang, 2012; and Yoo *et al.*, 2007).

Digital image sensors often develop defects over time, reducing the quality of the captured images (Chapman *et al.*, 2017). Fortunately, the degradation process is usually very slow (Pérez *et al.*, 2016). The most common type of image sensor defects is "hot pixels" (Chapman *et al.*, 2017

a)Author to whom correspondence should be addressed: Damien.Igoe@usq.edu.au

and Chapman *et al.*, 2016), which are considerably brighter than the surrounding pixels (Aranda *et al.*, 2017). Although imaging sensors are referred to as digital systems, the actual pixel portion is in reality an analog device, allowing a range of intensity values to be observed (Chapman *et al.*, 2017). The pixel intensity (brightness) is a function of the incident radiation rate, the dark noise, the dark current offset, and the duration of exposure. Dark noise and dark current offset should be close to zero for reliable measurements and any increase of the dark noise above typical noise will amplify the pixel brightness, creating "hot pixels" (Chapman *et al.*, 2017).

As dark noise images are not affected by any external illumination, its source originates from processes occurring within the image sensor and pixel structure itself. Dark noise is usually the product of thermally generated current generated by processes such as the Shockley-Read-Hall thermal free-minority carrier generation or recombination (Adão *et al.*, 2017 and Carrère *et al.*, 2014). Additionally, hot pixels have also been statistically found to be caused by cosmic radiation (Aranda *et al.*, 2017 and Chapman *et al.*, 2017).

Dark noise is the noise of the captured image with the image sensor being completely covered (Yoshida, 2006). Although there is evidence that the dark noise increases with increasing ambient temperature (Pérez *et al.*, 2016; Irie *et al.*, 2008; and Baer, 2006), recent research conducted by Igoe *et al.* (2014) indicated that smartphone image sensors are shielded from temperature changes. Dark noise distributions tend to exhibit a strong positive skew with a long tail, and the associated pixel values cannot be negative, hence lognormal distributions have been found to be a suitable model for the data (Igoe *et al.*, 2014 and Baer, 2006). Averaging all pixels across several images (Pereira, 2013) or recalibrating the sensor (Chapman *et al.*, 2017) can reduce only the random noise effects occurring in the image sensor array but not those effects resulting from other types of sensor defects (Chapman *et al.*, 2017). The random noise needs to be reduced to its minimum value at the beginning of imaging and before applying any further image filtering techniques in order to minimise noise propagation to successive image processing operations (Aranda *et al.*, 2017; Chapman *et al.*, 2017; Zhu and Huang, 2012; and Yoo *et al.*, 2007).

Different image filtering methods are applied to remove the undesirable dark noise effects from the sensor response, ensuring that the captured image results only from the true information of the image (Pérez *et al.*, 2016). Median filtering is a simple widely used non-linear, rank-order filter that is capable of attenuating the accompanying noise from the image while preserving its details (Aranda *et al.*, 2017; Tania and Rowaida, 2016; Zhu and Huang, 2012; and Patidar *et al.*, 2010). Hot-pixels are a visual symptom of "salt-and-pepper" or "impulsive" noise, which often contains bright and sometimes dead pixels (Aranda *et al.*, 2017; Tania and Rowaida, 2016; and Patidar *et al.*, 2010). By comparison, simple linear-based filtering methods, such as mean filtering or "smoothing," are adversely affected by the presence of anomalously high pixel intensities, such as is the case for hot pixels of any magnitude (Tania and Rowaida, 2016).

The noise-reducing performance of the median filter depends on the size and shape of the filtering mask and the time required to calculate its median value; the filtering mask is an $n \times n$ square array whose centre is positioned in the currently processed pixel, and therefore, n is an odd number (Aranda *et al.*, 2017 and Zhu and Huang, 2012). The noise reduction ability of the filter increases as the area of the square mask is increased, but with a reduction in image details, and vice versa (Zhu and Huang, 2012). The median filter works by replacing the central pixel of an $n \times n$ square array with the median value of all the pixels within the array (Fig. 1). This process is repeated across the entire image (Aranda *et al.*, 2017).

Despite its time complexity for larger sized arrays, median filtering is a very effective technique for reducing noise from digital images (Zhu and Huang, 2012) and is particularly useful in scientific applications where image quality and pixel sensitivity are important. Characterising image sensor defects is important especially as the pixel size is reduced to the 1-2 μm range (Chapman *et al.*, 2017). This research evaluates the use of median filtering in determining a dark noise threshold for high resolution smartphone image sensors.

METHOD

Equipment

A Sony Xperia Z1 smartphone (Sony Corporation, Tokyo, Japan) was employed, and the images comprised 5248 × 3936 pixels on a backside illuminated Exmor RS stacked image sensor with an active pixel area of approximately 27.48 mm^2. The high resolution comes from pixel sizes approaching 1 μm as described by Chapman *et al.* (2017). Dark noise images were recorded by placing black felt over the camera sensor

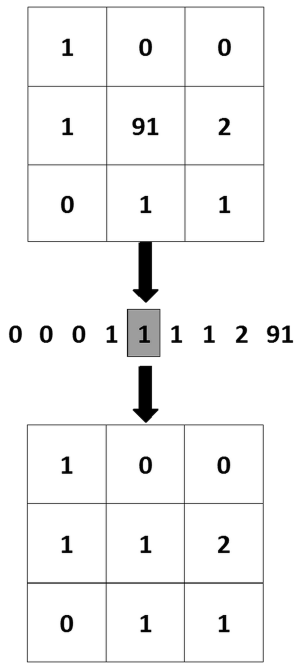

FIG. 1. Simplified median filtering used in this research. The central pixel in the top 3 × 3 array is anomalously high (hot pixel). It is eliminated by computationally taking the median of all pixel intensities in the square array (highlighted in the ordered list); this value then replaces the central anomalous pixel, as in the filtered array underneath (adapted from Aranda *et al.* 2017).

to prevent any light entering the sensor. Images were taken using default settings and saved in the default JPEG format. All images were captured in the default settings of the smartphone image sensor, and exhibited consistent settings in use, with a gain of ISO 800, an f-number of $f/2$, and an exposure time of 0.125 s.

Unlike previous object-detection-based image processing (Igoe *et al.*, 2017), dark noise images generally exhibit uniform low-intensity pixel values, far closer to their grayscale (Y) value than any hue (Sural *et al.*, 2002). Hence, all pixels were converted to their grayscale intensity values.

Grayscale pixel intensities were calculated using the luminance formula [Eq. (1)] comprising a known proportion of the red, green, and blue (RGB) signal from the image sensor (Wei *et al.*, 2016 and Alala *et al.*, 2014). Grayscale pixel intensities are measured in "digital numbers" (DN) that range from 0 to 255 for an 8-bit image sensor,

$$Y = 0.299R + 0.587G + 0.114B. \quad (1)$$

Data analysis and visualisation for this research were performed using the program language *Python* (version 3.5.2, python.org) and *Microsoft Excel*. The *Python* libraries used for data analysis and visualisation included the following:

1. *OpenCV*—used to read the image data and convert the pixels to grayscale values (Mistry and Saluja, 2016).
2. *NumPy*—to organise and manage the image array data (Abraham *et al.*, 2014 and Oliphant, 2007).
3. *SciPy*—used to define and apply the median filter (Oliphant, 2007).
4. *Matplotlib*—to generate graphs and specifically using *mpl_toolkits* to generate 3D graphs (Wood, 2015 and Abraham *et al.*, 2014).

Temperature effects

A dataset of 124 photos was taken as part of research by Igoe *et al.* (2017) with no illumination entering the image sensor (Chapman *et al.*, 2017), across ambient temperatures ranging from 5 °C to 25 °C during the field observations. Images were converted to grayscale (Igoe *et al.*, 2014) to ascertain the radiometric response value (Riutort-Mayol *et al.*, 2012). The temperature invariance observed in earlier dark noise observations (to 38 °C) by Igoe *et al.* (2014) was further tested in the current research, as a different and more modern smartphone was used than that in the earlier study. The root mean squared (RMS) error was calculated to confirm the consistency of the dataset. The defect rate which estimates the increase of defective pixels such as hot pixels over a period of time (Chapman *et al.*, 2017) was also determined.

Median filtering

The grayscale images were also used in median filter ranking of pixel values (Zhu and Huang, 2012). The geometric mean and standard deviation were calculated as pixel intensity distributions tended to be heavily positively skewed and the pixel values cannot be negative (Igoe *et al.*, 2014; Baer, 2006; and Limpert *et al.*, 2001). Geometric mean, standard deviation, and 6σ (6th standard deviation upper threshold representing 99.999%+ of background pixel values) were taken from the images, the latter used to indicate the maximum magnitude of the dark noise. Additionally, the maximum pixel intensity and a count of pixels with values greater than the threshold were taken ("hot pixels").

Median filters of different sizes were then applied with the same statistics calculated. Dark noise images do not possess any particular image features; the priority is on noise reduction (Zhu and Huang, 2012). A threshold was calculated at the inflection point on a plot of median filter size against 6σ where the maximum image pixel intensity is less than the 6σ-based threshold; all pixel intensities above this threshold are referred to as "hot pixels." Additionally, the time taken to execute the algorithm using different sized median filters was calculated to gauge the time complexity of each iteration (Zhu and Huang, 2012). A flowchart summarising the filtering process (after temperature effects are observed) is included in Fig. 2.

Further dark noise images were taken approximately a year later in June 2017 to test for any degradation of the image sensor due to use or aging. In addition, noise characteristics, especially of hot pixel occurrences, associated with all resolutions available on the Sony Xperia Z1 smartphone were also compared and analyzed. Available resolutions included 20.7 MP, 8.3 MP, 8.0 MP, 3.1 MP, and 2.1 MP, representing an increase in the effective pixel size, as the dimensions of the actual image sensor do not change. Furthermore, light-leaked images were also tested to determine if this phenomenon could be detected using this method.

Validation

To validate the developed method, it has been applied to four different phones with pixel sizes still within the 1-2 μm range. Two of the phones have image sensors and have the same manufacturer as the Sony Xperia Z1; these are the iPhone 6

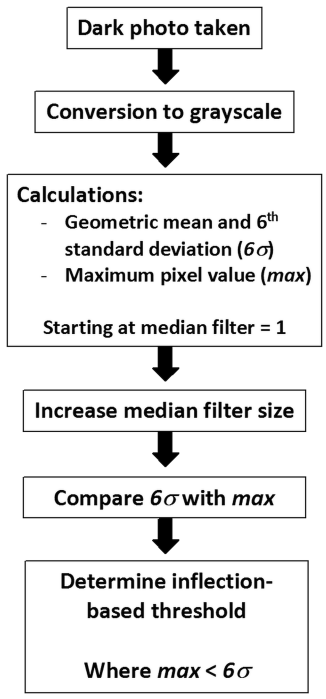

FIG. 2. The filtering and thresholding method developed in this research.

and the very recently released iPhone 8 plus, both using a Sony Exmor RS image sensor. A Samsung Galaxy S5 was also tested; the image sensor for this phone has isolated pixels, preventing crosstalk based noise (Fontaine, 2015). Finally, an older model smartphone, the LG Optimus G Pro, with previously identified image sensor damage from over-exposure to the sun was tested. The ambient temperatures were within the range tested initially.

RESULTS AND DISCUSSION

The overall average dark noise grayscale magnitude was 0.76 DN with a standard deviation of 1.81 DN. All 124 dark noise images had averages and standard deviations very similar to the overall value, with an RMS error not exceeding 0.004 for any image. The consistent settings result in an approximate pixel defect rate (Chapman *et al.*, 2017) of 1.43 pixels/mm^2/yr. This is equivalent to an increase of about 40 pixels for the sensor per year, which is a very low proportion of the image sensor; therefore, the mean dark noise is not expected to be changed significantly over many years of use. It is not possible to exactly predict when the image sensor response will become significantly different due to the random nature of how these defects present themselves (Chapman *et al.*, 2017).

Temperature effects

The analysis of the 124 dark images of 5248 × 3936 pixels each (20.7 MP) that were taken in ambient temperatures between 5 °C and 25 °C showed a negligible effect of temperature on the dark noise. The variation in ambient temperature resulted in no significant increase in image sensor dark noise geometric mean (Fig. 3), consistent with earlier observations by Igoe *et al.* (2014). The same ambient temperature shielding assumption was applied to the phone cameras used for the validation phone camera models.

Median filtering

An important factor in the use of median filters is the time it takes the software to perform filtering across the entire image. The Python-based *time* function was used to investigate the change of filtering process time with increasing median filter sizes. As the median filter was increased, the processing time increased exponentially, from approximately half a second for the raw image to over a minute for a filter with a side length of 15 pixels, taking over 100 times longer to process than the original image. The latter placed a significant time cost on analyses involving multiple images.

A sample image from the 124 dark images was selected due to its geometric mean and standard deviation being very similar to the overall values, with an RMS error of approximately 3.25×10^{-5}. When the image was analyzed for the number and the maximum grayscale pixel intensity (digital number) of hot-pixels, and the 6σ value for sequential median filters up to a size 15 (15 × 15 grid), the inflection point where the maximum pixel value fell below the 6σ value was found to occur at an intensity of approximately 9 DN (Fig. 4)—for the purposes of analysis, all pixel intensities above this value are referred to as "hot pixels." The optimum median filter size was surmised to be 7 (i.e., a 7 × 7 median filter), where the maximum pixel grayscale intensity value was less than the 6σ upper boundary (Fig. 4).

The original image possessed 10 348 hot pixels that were distributed randomly and represented about 0.05% of the total pixels of the image. A sample of 500 × 500 pixels of the original image is presented in 3D structure in Fig. 5(a). In comparison, the same section is shown in Fig. 5(b) after a size 7 median filter has been applied, removing all hot pixels.

For the further images taken over eight months of almost continuous solar UV smartphone imaging on a series of field campaigns, although there was an overall increase in the geometric mean and standard deviation (0.85 DN and 1.71 DN, respectively), the pattern in a representative image remained almost the same as the original image (Fig. 4). Some of the increase in mean and standard deviation could be attributed to an approximate 10% increase in hot pixels appearing in the new unfiltered image, possibly due to residual thermal effects from the extensive field use and exposure to direct sun. There was no appreciable difference in the magnitude of the 6σ-inflection threshold and the location of the inflection.

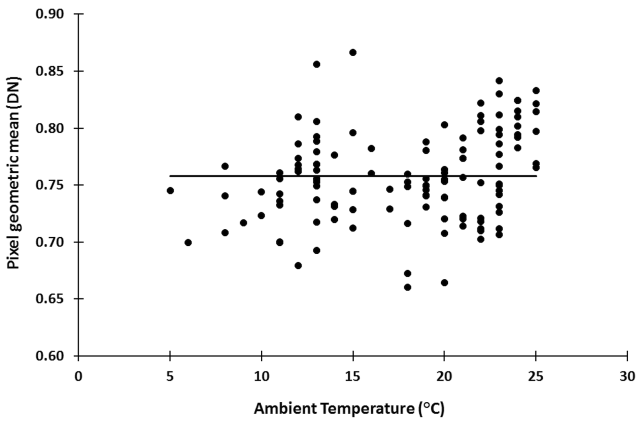

FIG. 3. Geometric mean of the pixel values of 20.7 megapixels for each data point in response to varying ambient temperatures. The line represents the mean of the 124 data points.

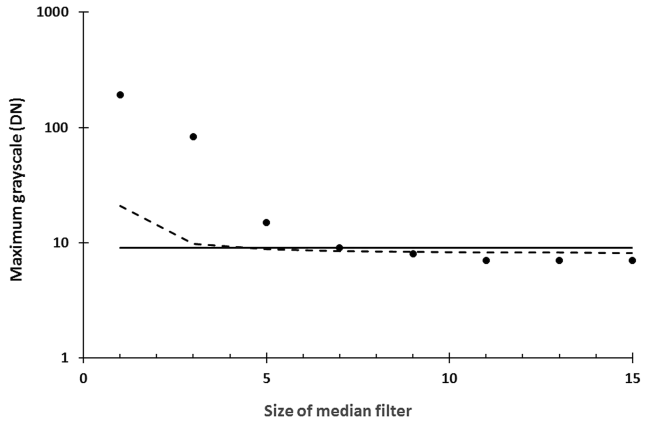

FIG. 4. Maximum grayscale pixel intensity value (dots) and the 6th upper standard deviation (dashed line) for a sample dark image, from the original image (median filter size = 1) to a median filter of size 15. The 6σ-inflection threshold is shown as a black line.

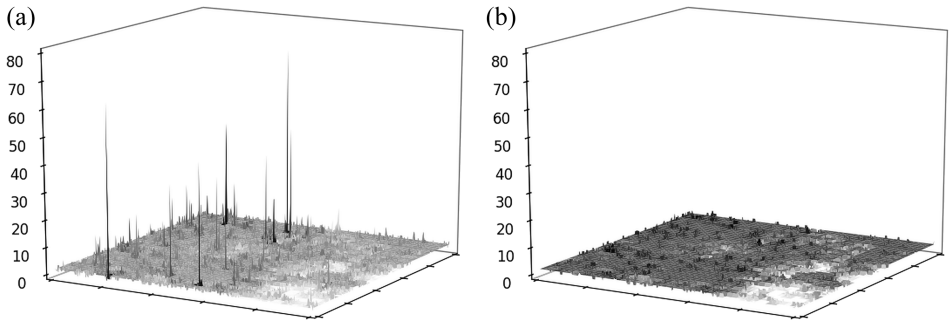

FIG. 5. (a) 3D visualisation of a 500 × 500 pixel section of the original sample image. Hot pixels are shown as spikes. The vertical scale is the grayscale pixel intensity in digital numbers (DN). (b) The same section as in (a) having been filtered by a 7 × 7 median filter. All hot pixels have been successfully removed, as seen by the absence of sharp spikes.

Resolution

The smartphone used (Sony Xperia Z1) has four additional lower resolution imaging options from the main 20.7 MP default. Resolutions of 8.3 MP, 8.0 MP, 3.1 MP, and 2.1 MP are available for smartphone photography, the video recording setting was not considered in this research. Additionally, a front-facing camera is available with a resolution of 2.1 MP; however, several images taken with this camera were extremely noisy, suggesting that it may be defective, thus was also not used.

The analysis of a series of dark images that were taken using each of the available resolutions indicated a strong correlation between the resolution and dark noise (Table I). The geometric mean decreased logarithmically with decreasing resolution. The geometric standard deviations tended to remain fairly consistent. Every image possessed the same gain, f-number, and exposure times as the original samples.

The reduction in the geometric mean and maximum pixel intensity is due to a larger effective pixel area, with the hot pixel intensities present at higher resolutions being averaged or "smoothed" out with the intensities of neighbouring pixels.

A similar pattern of maximum pixel intensity values and the upper 6σ boundary was observed for the different resolutions when median filters (up to size 15) were applied (Fig. 6). The inflection-based threshold was found to be the same as the original characterisation data, 9 DN.

A similar, almost parallel trend is visible for all resolutions, with all allowing an inflection-based threshold at the same amount. A major difference is that the optimum dimensions of the median filter decrease as the resolution decreases, from size 7 for the 20.7 MP image, size 5 for the 8.3 MP and 8.0 MP images, and size 3 for the 3.1 MP and 2.1 MP images.

TABLE I. Comparison of the geometric mean and standard deviation, and maximum pixel intensity for the resolutions available in the Sony Xperia Z1 smartphone.

Resolution (MP)	Geometric mean (DN)	Geometric standard deviation (DN)	Maximum pixel intensity (DN)
20.7	0.85	1.71	239
8.3	0.82	1.66	113
8.0	0.81	1.66	102
3.1	0.75	1.68	55
2.1	0.65	1.72	29

Hot pixel analysis

Further analysis of the effects of temperature on the original characterisation showed a moderate linear correlation between the ambient temperature and the number of hot pixels (Fig. 7), as defined earlier as being above the inflection-threshold (9 DN). However, the increase in hot pixel occurrences as the temperatures increased was not sufficient to significantly alter the overall geometric mean and standard deviations for the dark images (as the total amount of hot-pixels represent 0.1% or less of the total number of pixels

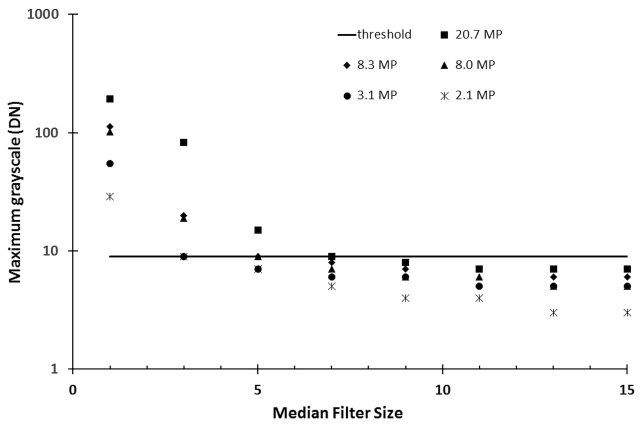

FIG. 6. Comparison between dark images from different resolutions when median filters of different sizes are applied.

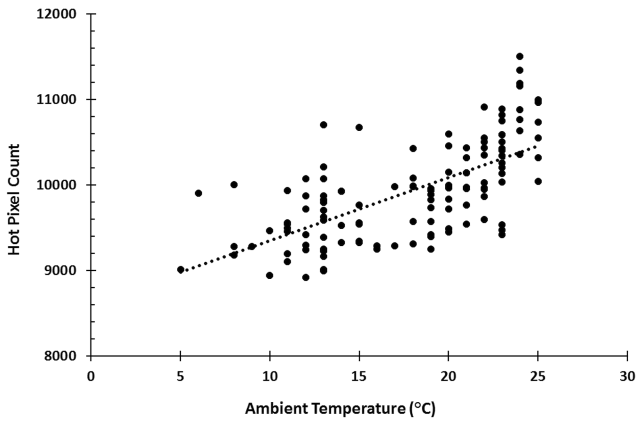

FIG. 7. Hot pixel count with increasing temperature for the original 124 dark images.

TABLE II. Comparison of hot pixel count and maximum hot pixel intensity values for the resolutions available in the Sony Xperia Z1 smartphone.

Resolution (MP)	Hot pixel count	Maximum hot pixel intensity (DN)
20.7	11 389	239
8.3	1 700	113
8.0	1 583	102
3.1	394	55
2.1	80	29

in the image), consequently resulting in the overall temperature invariance observed in Fig. 3. The magnitude of the "hottest" hot pixel did not demonstrate any temperature-based variation.

The resolution of the image is also a significant factor in both the amount and intensity of hot pixels (Table II). There is a roughly parabolic increase in the amount and magnitude of hot pixels as the resolution increases.

The method developed performed efficiently for all resolutions irrespective of the number of hot pixels that were observed to be present.

Light leakage

Another source of error from collected dark noise images is light leakage. Two sample light leaked images were compared to the original dark image: one was slightly light-leaked (non-visible with a higher geometric mean of 3.4 DN) and the second was visibly light-leaked (geometric mean of 28.5 DN).

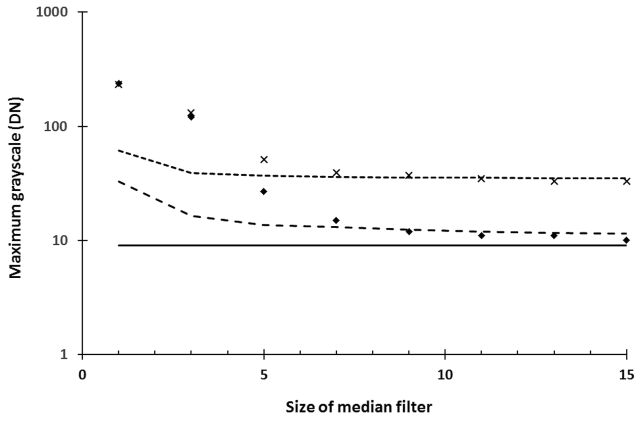

FIG. 8. Comparison of the maximum pixel values and the 6th upper standard deviation for sub-visible light leakage (diamonds and dashed line, respectively) and for a visibly light-leaked image (crosses and short-dashed line, respectively). The earlier developed 6σ-inflection threshold (black line) is shown for comparison.

A significant observation is that the maximum intensity values for both are comparable to non-light leaked images when unfiltered; this is particularly important for the situation where light leakage is not entirely visible, potentially resulting in incorrect statistical information about the image sensor's dark noise properties.

Once different sized median filters were applied (Fig. 8), the differences between the light-leaked images and the original image became more apparent with the remaining maximum values and the 6σ-inflection threshold almost entirely translated to higher values proportional to the magnitude of

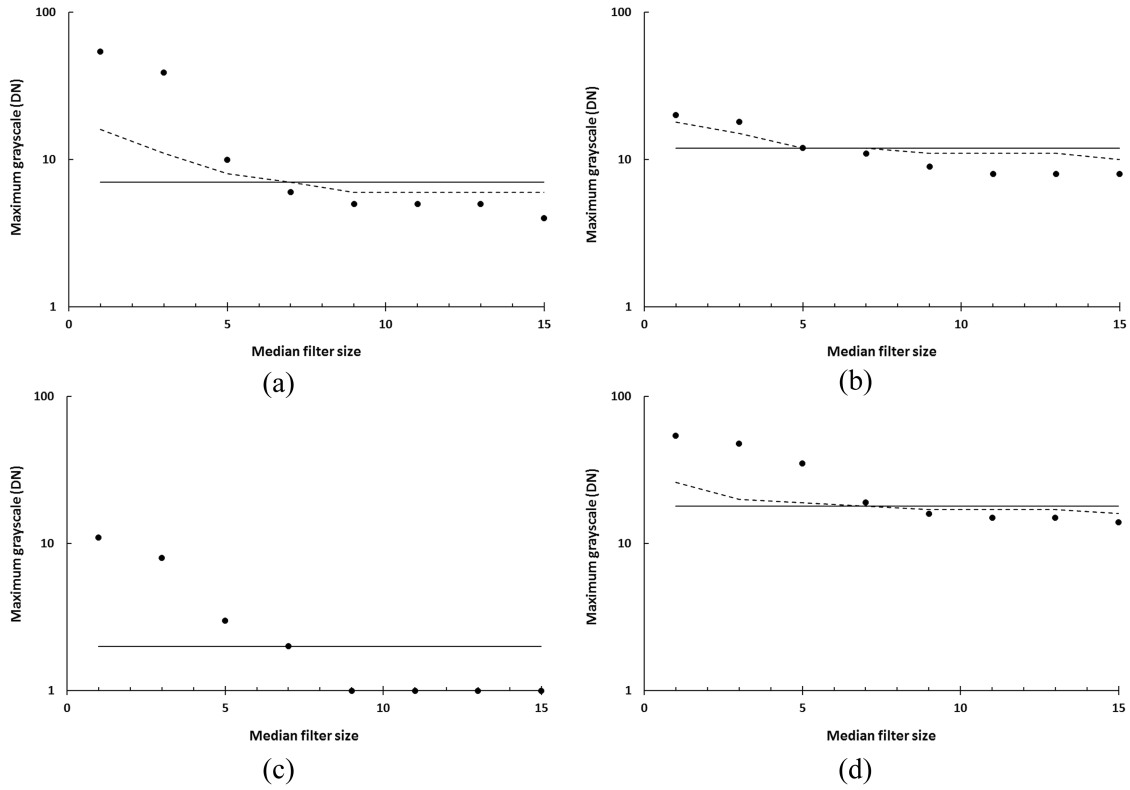

FIG. 9. (a) Dark noise and hot pixel characteristics of the iPhone 6. (b) Dark noise and hot pixel characteristics of a Samsung Galaxy S5. (c) Dark noise and hot pixel characteristics of an iPhone 8 plus. (d) Dark noise and hot pixel characteristics of a LG Optimus G Pro with a damaged image sensor.

the intensity of the light leakage. However, the inflection point remained in the same approximate position.

As the light leaked images are translations of the true dark images, it may be possible to use this type of analysis to mathematically correct for light leakage; however, further study would be needed to determine the effectiveness and robustness of such a method.

Validation

Modeling of the dark noise and hot pixel characteristics of the four additional phone cameras are compared in Figs. 9(a)–9(d). All display similar general characteristics as that observed for the Sony Xperia Z1. Different thresholds were observed, very likely due to differences in the architecture within the phone and image sensors; however, there were very little differences in the optimum median filter size. The dark noise and hot pixel characteristics of the iPhone 6 were the most similar [Fig. 9(a)].

The Samsung Galaxy S5 noise characteristics were very similar to the Sony, but the hot pixel intensities were considerably lower, closer to the 6σ line [dashed line—Fig. 9(b)]. This could be due to the "deep trench isolation" technology used in the image sensor (Fontaine, 2015), suggesting that a potential cause of hot pixel intensities may be due to electrical and optical crosstalk in the substrate that this technology prevents.

The iPhone 8 plus is a very new model at the time of writing this paper. All noise and hot pixel parameters are considerably lower than any other phone camera tested [Fig. 9(c)], suggesting significant advances in noise suppression.

The LG Optimus G Pro had previously been identified to have a damaged image sensor, with consistently elevated noise levels [Fig. 9(d)]. Despite the damage, the overall pattern observed remains similar to the Sony Xperia Z1, displaying traits similar to that observed for non-visible light leakage (refer to Fig. 8). As both light leakage and damaged image sensors are deleterious to any high precision observations, it is not relevant to be able to distinguish between them.

CONCLUSION

Throughout this paper high resolution smartphone images were explored via dark noise analysis. An increase in image noise was seen with higher resolutions, in particular, an increase in the number of hot pixels, and a lognormal distribution was found to be a suitable model for this data. It was also found that the mean pixel intensity of dark noise images did not vary significantly with ambient temperatures between 5 °C and 25 °C. The slight increase in hot-pixel occurrences with temperature represented 0.1% or less of the total amount of pixels in an image, so the effects of these were negligible.

Median filtering techniques were effectively employed to reduce noise associated with the high-resolution Sony Xperia Z1 smartphone image sensor which has a dark noise threshold of about 9 DN. The processing time increased exponentially as the median filter size was increased, with a surmised optimum filter size of 7×7; similar patterns were observed for an iPhone 6, iPhone 8 plus, Samsung Galaxy S5 and a damaged LG Optimus G Pro. The use of median filtering also made light leakage more apparent when compared to the original images. From the data analysis and visualisation gathered from *Python* and *Microsoft Excel*, the overall average dark noise grayscale magnitude was 0.76 DN with a standard deviation of 1.81 DN, and this mean is not expected to change significantly over many years of use due to the low defect rate of 1.43 pixels/mm^2/yr.

The available resolutions of 20.7 MP, 8.3 MP, 8.0 MP, 3.1 MP, and 2.1 MP were also tested. The geometric mean of the pixel values of these lower resolutions was found to decrease logarithmically as the resolution was decreased and effective pixel size is increased. The inflection-based threshold was determined to be 9 DN for each resolution, which was the same as the original characterisation data. As the resolutions were increased, a roughly parabolic increase in the amount and magnitude of hot pixels was also seen. These results show the versatility of smartphones, in particular, the proliferation of in-built high resolution cameras, for low-cost and easy-to-use scientific applications.

Abraham, A., Pedregosa, F., Eickenberg, M., Gervais, P., Mueller, A., Kossaifi, J., Gramfort, A., Thirion, B., and Varaquaux, G., "Machine learning for neuroimaging using scikit-learn," Front. Neuroinf. **8** (2014).

Adão, T., Hruška, J., Padua, L., Bessa, J., Peres, E., Morrais, R., and Sousa, J. J., "Hyperspectral imaging: A review on UAV-based sensors, data processing and applications for agriculture and forestry," Remote Sens. **9**, 1110 (2017).

Alala, B., Mwangi, W., and Okayo, G., "Image representation using RGB color space," Int. J. Innovative Res. Dev. **3**, 322–328 (2014), ISSN: 2278-0211.

Aranda, L. A., Reviriego, P., and Maestro, J. A., "Error detection technique for a median filter," IEEE Trans. Nucl. Sci. **64**, 2219–2226 (2017).

Baer, R., "A model for dark current characterization and simulation," Proc. SPIE **6068**, 37–48 (2006).

Batistell, G., Zhang, V. C., and Sturm, J., "Color recognition sensor in standard CMOS technology," Solid-State Electron. **102**, 59–68 (2014).

Carrère, J.-P., Oddou, J.-P., Benoit, D., and Roy, F., "CMOS image sensor process impact on dark current," in *IEEE International Reliability Physics Symposium* (IEEE, 2014).

Chapman, G. H., Thomas, R., Coelho, K., Meneses, S., Yang, T., Koren, I., and Koren, Z., "Increases in hot pixel development rates for small digital pixel sizes," Electron. Imaging **6**, 1–6 (2016).

Chapman, G. H., Thomas, R., Koren, I., and Koren, Z., "Hot pixel behaviour as pixel size reduces to 1 micron," in *IS&T International Symposium on Electronic Imaging 2017: Image Sensors and Imaging Systems* (Society for Image Science and Technology, 2017), pp. 39–45.

Fontaine, R., "The state-of-the-art of mainstream CMOS image sensors," in *Proceedings of the International Image Sensors Workshop*, pp. 6–12 (2015).

Fung, C. H. and Wong, M. S., "Improved mobile application for measuring aerosol optical thickness in ultraviolet-A wavelengths," IEEE Sens. J. **16**, 2055–2059 (2016).

Hussain, I., Ahamad, K. U., and Nath, P., "Water turbidity sensing using a smartphone," RSC Adv. **6**, 22374–22382 (2016a).

Hussain, I., Ahamad, K. U., and Nath, P., "Low-cost, robust, and field portable smartphone platform photometric sensor for fluoride level detection in drinking water," Anal. Chem. **89**, 767–775 (2016b).

Hussain, I., Das, M., Ahamad, K. U., and Nath, P., "Water salinity using a smartphone," Sens. Actuators, B **239**, 1042–1050 (2017).

Igoe, D. P., Parisi, A. V., and Carter, B., "A method for determining the dark response for scientific imaging with smartphones," Instrum. Sci. Technol. **42**, 586–592 (2014).

Igoe, D. P., Amar, A., Parisi, A. V., and Turner, J., "Characterisation of a smartphone image sensor response to direct solar 305 nm irradiation at high airmasses," Sci. Total Environ. **587-588**, 407–413 (2017).

Irie, K., McKinnon, A., Unsworth, K., and Woodhead, I., "Measurement of digital camera image noise for imaging applications," Sens. Transducers **90**, 185–194 (2008), ISSN: 1726-5479.

Lee, S., Kim, J., Jin, C., Bae, S., and Choi, C., "Assessment of smartphone-based technology for remote environmental monitoring and its development," Instrum. Sci. Technol. **40**, 504–529 (2012).

Limpert, E., Stahel, W. A., and Abbt, M., "Log-normal distributions across the sciences: Keys and clues," BioScience **51**, 341–352 (2001).

Mistry, K. and Saluja, A., "An introduction to OpenCV using Python with Ubuntu," Int. J. Sci. Res. Comput. Sci., Eng. Inf. Technol. **1**, 65–68 (2016), ISSN: 2456-3307.

Oliphant, T. E., "Python for scientific computing," Comput. Sci. Eng. **9**, 10–20 (2007).

Park, Y. M., Han, Y. D., Chun, H. J., and Yoon, H. C., "Ambient light-based optical biosensing platform with smartphone-embedded illumination sensor," Biosens. Bioelectron. **93**, 205–211 (2017).

Patidar, P., Gupta, M., Srivastava, S., and Nagawat, A. K., "Image de-noising by various filters for different noise," Int. J. Comput. Appl. **9**, 45–50 (2010).

Pereira, E. S., "Determining the fixed pattern noise of a CMOS sensor: Improving the sensibility of autonomous star trackers," J. Aerosp. Technol. Manage. **5**, 217–222 (2013).

Pérez, M., Lipovetzky, J., Haro, M. S., Sidelnik, I., Blostein, J. J., Bessia, F. A., and Berisso, M. G., "Particle detection and classification using commercial off the shelf CMOS image sensors," Nucl. Instrum. Methods Phys. Res., Sect. A **827**, 171–180 (2016).

Präkel, D., *The Visual Dictionary of Photography* (Bloomsbury Academic, 2010).

Riutort-Mayol, G., Marques-Mateu, A., Segui, A. E., and Lerma, J. L., "Grey level and noise evaluation of a Foveon X3 image sensor: A statistical and experimental approach," Sensors **12**, 10339–10368 (2012).

Sural, S., Qian, G., and Pramanik, S., "Segmentation and histogram generation using the HSV color space for image retrieval," in International Conference on Image Processing, Rochester, USA, 2002.

Tania, S. and Rowaida, R., "A comparative study of various image filtering techniques for removing various noisy pixels in aerial images," Int. J. Signal Process., Image Process. Pattern Recognit. **9**, 113–124 (2016).

Turner, J., Parisi, A. V., Igoe, D. P., and Amar, A., "Detection of ultraviolet B radiation with internal smartphone sensors," Instrum. Sci. Technol. **45**, 618–638 (2017).

Wei, Q., Nagi, R., Sadeghi, K., Feng, S., Yan, E., Ki, S. J., Caire, R., Tseng, D., and Ozcan, A., "Detection and Spatial Mapping of Mercury Contamination in Water Samples using a Smartphone," ACS Nano **8**, 1121–1129 (2014).

Wei, C., Song, Y., and Lin, C., "Design of a solar tracking system using the brightest region in the sky image sensor," Sensors **26**, 1995 (2016).

Wood, M. A., "Making plots with matplotlib," in *Python and Matplotlib Essentials for Scientists and Engineers* (Morgan and Claypool Publishers, 2015).

Yetisen, A. K., Martinez-Hurtado, J. L., Garcia-Melendrez, A., da Cruz Vasconcellos, F., and Lowe, C. R., "A smartphone algorithm with inter-phone repeatability for the analysis of colorimetric tests," Sens. Actuators, B **196**, 156–160 (2014).

Yoo, Y., Lee, S., Choe, W., and Kim, C., "CMOS image sensor noise reduction method for image signal processor in digital cameras and camera phones," in *Digital Photography III*, edited by Martin, R. A., DiCarlo, J. M., and Sampat, N. (SPIE, 2007).

Yoshida, H., "Evaluation of image quality," in *Image Sensors and Signal Processing for Digital Still Cameras*, edited by Nakamura, J. (Taylor and Francis CRC, Boca Raton, USA, 2006).

Zhu, Y. and Huang, C., "An improved median filtering algorithm for image noise reduction," Phys. Procedia **25**, 609–616 (2012).